On the effect of acceleration on trailing edge noise radiation from rotating blades

S. Sinayoko[*]

Department of Engineering, University of Cambridge

M. Kingan[†]

Institute of Sound and Vibration, University of Southampton

A. Agarwal [‡]

Department of Engineering, University of Cambridge

For a rotating blade, classical theories of trailing edge noise neglect the blade acceleration; this assumption is thought to be valid when the frequency of the source is large compared to the angular velocity of the blade. This paper suggests that this assumption is more widely applicable. Acceleration is found to have a negligible effect on the average power spectral density even at low frequencies. This result is obtained by comparing the classical approach to two analytical formulations that take into account the acceleration of the blade. The formulations are applied to two model blade elements that are representative of a typical propeller at cruise and during take-off. An explanation for why the acceleration can be neglected at low frequencies is proposed.

Introduction

The generation of trailing edge noise can be modelled by means of a distribution of dipoles representing loads over the blade surface. These dipoles are induced by the scattering of hydrodynamic waves at the trailing edge.[1,2] As each dipole rotates with the blade, noise is generated through two different mechanisms:[3] the unsteadiness of the dipole itself; its acceleration due to the blade rotation. The latter effect scales[4] with the rotational speed Ω of the rotor, while the former scales with the source frequency ω'. This explains

[*]Research Associate, Department of Engineering, University of Cambridge
[†]Lecturer, ISVR, University of Southampton
[‡]Lecturer, Department of Engineering, University of Cambridge

why the effect of acceleration is neglected at high frequency ($\omega' \gg \Omega$) in the frequency domain approach of Schlinker and Amiet,[5] wherein each blade element is assumed to be in uniform translational motion.

Blandeau and Joseph[6] have explored the range of validity of Schlinker and Amiet's approach. They found that there was a low frequency limit and a high frequency limit, beyond which the approach of Schlinker and Amiet was no longer valid. However, Sinayoko et al[7,8] found that the implementation of Blandeau and Joseph differed significantly from that of Schlinker and Amiet. Furthermore, their approach did not take into account the effect of the mean flow on sound propagation, which are significant for high speed propeller blades. Thus the range of validity of Schlinker and Amiet's approach remains unclear.

The aim of this paper is to clarify this issue by comparing the approach of Schlinker and Amiet to several alternative formulations that take into account the effect of blade acceleration. One of these formulations is based on the work of Sinayoko et al.[7] It assumes that the source frequency is relatively large so that the spanwise correlation length is small, so it may not be sufficiently accurate to explore the validity of Schlinker and Amiet's approach to lower frequencies. Furthermore, it relies on Amiet's high frequency blade response function which becomes inaccurate when the source frequency blade response function small as would be the case for high speed propellers. To overcome these limitations, we have derived two alternative formulations for the simpler problem of a rotating dipole source. The first one combines the approach of Schlinker and Amiet[5] to the far field expression of Amiet[1] for a rotating dipole; it neglects the effect of acceleration. The second one is an exact solution of the Ffowcs-Williams and Hawkings equation that takes into account the effect of acceleration. No assumption is made in deriving this second formulation, so it will allow us to validate the approach of Schlinker and Amiet accurately over a broad frequency range.

The formulations discussed in the above paragraph focus on the power spectral density (PSD). For a rotating blade, the PSD is a function of both time and frequency: because of the Doppler effect, the PSD varies with the angular position of the blade around the hub.[?,9] This paper will therefore make the distinction between the time averaged PSD and the instantaneous PSD. The instantaneous PSD will provide a detailed picture of the impact of the acceleration term on the radiating sound field.

The structure of the paper is as follows. Background equations for trailing edge radiation from an isolated airfoil are given in §I. The formulations that include the effect of acceleration are derived in §II. The approach of Schlinker and Amiet,[5] which excludes the effect of acceleration is described in §III. The results and discussions are presented in sections IV and V respectively.

I. Trailing edge noise theory for isolated aerofoils

Consider a flat plate in a uniform flow of Mach number M_X at zero angle of attack. The observer location is expressed using a cartesian coordinate system (X, Y, Z), with X in the chordwise direction and pointing

downstream and Z in the vertical direction. According to Amiet,[1,10] the PSD at frequency ω is of the form

$$S_{pp}(\omega) = \left(\frac{\omega}{c_0}\frac{Z}{4\pi\sigma^2}\right)^2 S_{ff}(\omega), \tag{1}$$

where S_{ff} is a frequency force power spectral density,

$$\sigma^2 = X^2 + \beta^2(Y^2 + Z^2), \qquad \beta^2 = 1 - M_X^2, \qquad U_c = 0.8 M_X c_0, \tag{2}$$

where $U_c = 0.8U$ denotes the convection velocity of an eddy in the boundary layer near the trailing edge.

A. Distributed source model

For a stationary flat plate in a uniform flow,[11]

$$S_{ff}(\omega) = \frac{1}{2} S C^2 |\Psi_L(k_X, k_S, k_C)|^2 l_S(k_X, k_S) S_{qq}(\omega), \tag{3}$$

where S and C denote the blade span and chord,

$$k_X = \frac{\omega}{U_c}, \qquad k_S = \frac{\omega}{c_0}\frac{Y}{\sigma}, \qquad k_C = \frac{\omega}{c_0\beta^2}\left(M_X - \frac{X}{\sigma}\right), \tag{4}$$

and the correlation length l_S is derived as follows from the expression of Roger and Moreau[12]

$$l(k_X, k_S) \equiv \frac{1}{k_X}\frac{\eta}{\eta^2 + (k_S/k_X)^2}, \tag{5}$$

where η is the exponential decay rate of the spanwise coherence function. This paper will use the value $\eta = 0.62$ measured by Brooks et al[13] for a NACA 0012 at Mach 0.11 and zero angle of attack. When k_X tends to 0, the expression of equation (5) becomes very large so for a given blade of span S, following the approach of Kim and George,[14] we will define the spanwise correlation length as

$$l_S(k_X, k_S) \equiv \frac{S}{1 + S/l(k_X, k_S)}. \tag{6}$$

The acoustic lift Ψ_L is defined as

$$\Psi_L(k_X, k_S, k_C) = \frac{i}{A}\left\{\frac{\sqrt{iB}}{\sqrt{iB - iA}}\mathrm{erf}\Big(\sqrt{2(iB - iA)}\Big) + e^{i2A}\left[1 - \mathrm{erf}\Big(\sqrt{2iB}\Big)\right]\right\}, \tag{7}$$

$$A = \overline{k}_X + \overline{k}_C, \qquad B = \overline{k}_X + \overline{\kappa} + M_X\overline{\mu}, \qquad \mu = M_c k_X/\beta^2, \tag{8}$$

where the overbar denotes normalisation by $C/2$ and M_c is the convective Mach number near the trailing edge. The wavenumber κ is a function of the spanwise wavenumber k_S:

$$\kappa \equiv \begin{cases} \mu\sqrt{1 - k_S^2/(\beta\mu)^2} & \text{if} \quad k_S^2 < (\beta\mu)^2 \\ -i|\mu|\sqrt{k_S^2/(\beta\mu)^2 - 1} & \text{if} \quad k_S^2 \geq (\beta\mu)^2 \end{cases} \tag{9}$$

The PSD of the incoming pressure fluctuations at the trailing edge, denoted $S_{qq}(\omega)$, can be measured experimentally. If no experimental data is available, it can be estimated by using empirical low-order models. These low order models are expressed in terms of parameters characterising the boundary layer, such as the boundary layer thickness, displacement thickness, wall shear stress etc. A review of the different models is given by.[15] This paper uses the model of,[16] i.e.:

$$S_{qq}(\omega) = \left(\frac{1}{2}\rho U_X^2\right)^2 \frac{\delta^*}{U_X} F(\overline{\omega}), \tag{10}$$

where $\overline{\omega} = \omega\delta^*/U_X$ and δ^* is the boundary layer displacement thickness defined as

$$\delta^* = \begin{cases} c(24.3 + 0.6625\chi) \times 10^{-4}, & \text{if} \quad \chi \leq 4^\circ \\ c(26.95 + 0.6625(\chi - 4) + 0.3044(\chi - 4)^2 + 0.0104(\chi - 4)^3) \times 10^{-4}, & \chi > 4^\circ. \end{cases} \tag{11}$$

in terms of the angle of attack χ, and

$$F(\overline{\omega}) = \begin{cases} \dfrac{1.732 \times 10^{-3}\overline{\omega}}{1 - 5.489\overline{\omega} + 36.74\overline{\omega}^2 + 0.1505\overline{\omega}^5} & \text{if} \quad \overline{\omega} < 0.06, \\ \dfrac{1.4216 \times 10^{-3}\overline{\omega}}{0.3261 + 4.1837\overline{\omega} + 22.818\overline{\omega}^2 + 0.0013\overline{\omega}^3 + 0.0028\overline{\omega}^5} & \text{if} \quad \overline{\omega} \geq 0.06. \end{cases} \tag{12}$$

B. Point source model

For a point source model, we ignore the scattering of the incoming turbulent gusts a the trailing edge encapsulated by the acoustic lift Ψ_L and model the force spectrum as

$$S_{ff}(\omega) = C^2 S l_S(k_X, k_S) S_{qq}(\omega), \tag{13}$$

where S_{qq} and l_S are defined in equations (10) and (6) respectively.

II. Trailing edge noise formulation for a rotating blade including acceleration effects

A. Exact formulation for a rotating dipole

Instantaneous power spectral density

The instantaneous PSD is defined in the frequency domain as

$$S_{pp}(\mathbf{x_o}, t, \omega) = \int_{-\infty}^{+\infty} \tilde{R}_{pp}(\mathbf{x_o}, \omega, \nu) e^{i\nu t}\, d\nu, \tag{14}$$

where $\tilde{R}_{pp}$ is the frequency autocorrelation function defined as

$$\tilde{R}_{pp}(\mathbf{x_o}, \omega, \nu) = E[\tilde{p}(\mathbf{x_o}, \omega + \nu/2)\tilde{p}^{\star}(\mathbf{x_o}, \omega - \nu/2)], \tag{15}$$

where $\tilde{p}$ denotes the Fourier transform of p over time:

$$\tilde{p}(\mathbf{x}_o, \omega) = \frac{1}{2\pi} \int_{-\infty}^{+\infty} p(\mathbf{x}_o, t) e^{-i\omega t}\, dt. \tag{16}$$

An expression for $\tilde{p}(\mathbf{x_o}, \omega)$ can be derived using Garrick and Watkin's Green's function leading to[7,8]

$$\tilde{p}(\mathbf{x_0}, \omega) = i\tilde{g} \sum_{n=-\infty}^{+\infty} e^{-in(\gamma_0 - \pi/2)} \int_{\Sigma} \int_{R_h}^{R_t} k_L J_n(k_r r') \tilde{L}(\omega - n\Omega, X, r') e^{ik_z z}\, dX\, dr', \tag{17}$$

where γ_0 is the observer azimuthal angle, $\tilde{L}$ is the lift force per unit surface, X is the distance from the trailing edge, and

$$\tilde{g} = \frac{e^{-ikR_e}}{4\pi R_e(1 - M_z \cos\theta_e)} \qquad k_L = k_z \cos\alpha - \frac{n \sin\alpha}{r'}, \qquad k_z = \frac{k\cos\theta_e}{1 - M_z\cos\theta_e}, \qquad k_r = \frac{k\sin\theta_e}{1 - M_z\cos\theta_e}, \tag{18}$$

where $k = \omega/c_0$ and we have introduced the spherical emission coordinates R_e and θ_e which measure the distance and elevation of the observer from the convected (or retarded) source position $\mathbf{x_c} = -M_z c_0 T_e$ (figure 1), with T_e the time it takes for sound to propagate from the source to the observer. For a point source we can assume $\tilde{L} = \delta(X)\delta(r - a)\tilde{F}(\omega)$ so

$$\tilde{p}(\mathbf{x_0}, \omega) = \frac{i}{4\pi R_e(1 - M_z\cos\theta_e)} \sum_{n=-\infty}^{+\infty} e^{-in(\gamma_0 - \pi/2)} k_L J_n(k_r r) \tilde{F}(\omega - n\Omega) e^{ik_z z}, \tag{19}$$

where k_L is evaluated at $r' = r$.

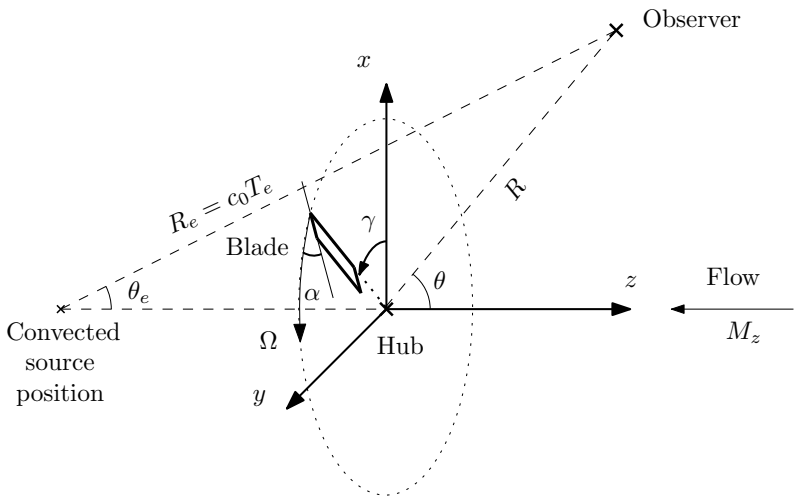

Figure 1: Stationary observer in a uniform flow. The reference frame is attached to the hub around which a blade element is rotating at angular velocity Ω. For an obsever in the far field, the source can be assumed to be located at the hub so the convected source position is as located downstream of the hub at $\mathbf{x_c} = -M_z c_0 T_e$.

Substituting (19) into (14) we find

$$S_{pp}(\mathbf{x_o}, t, \omega) = \frac{1}{(4\pi R_e(1 - M_z \cos\theta_e))^2} \sum_{m=-\infty}^{+\infty} \sum_{n=-\infty}^{+\infty} e^{im(\Omega(t-R_e/c_0)-\gamma_o+\pi/2)} \\ k_L k'_L J_n(k_r r) J_{n+m}(k'_r r) S_{ff}(\omega - [m/2+n]\Omega), \quad (20)$$

where the primed wavenumbers are a function of frequency $\omega + m\Omega/2$ and the non-primed ones of $\omega - m\Omega/2$, and where we have used the relationship $S_{ff}(\omega) = E[|\tilde{F}(\omega)|^2]$. The force frequency spectrum will be computed from equation (13).

Time averaged power spectral density

The time averaged PSD can be obtained by time averaging equation (20). The modes $m \neq 0$ do not contribute to the average so

$$\overline{S}_{pp}(\mathbf{x_o}, \omega) = \frac{1}{(4\pi R_e(1 - M_z \cos\theta_e))^2} \sum_{n=-\infty}^{+\infty} k_L^2 J_n^2(k_r r) S_{ff}(\omega - n\Omega). \quad (21)$$

B. Approximate formulation for a distribution of dipoles

An analytical formulation for trailing edge radiation from a rotating thin blade element has been derived by Sinayoko et al,[7,8] for both the instantaneous PSD and the time averaged PSD. The main results are summarized below.

Instantaneous PSD

At high frequency, for a small blade element of span S that is large compared to the spanwise correlation length, the far field instantaneous PSD for trailing edge noise is given by

$$S_{pp}(\mathbf{x_o},\omega,t) = S\sum_{m=-\infty}^{+\infty}\frac{e^{-im(\Omega R_e/c_0+\gamma_o-\pi/2)}}{\left[8\pi R_e(1-M_z\cos\theta_e)\right]^2}\left(\sum_{n=-\infty}^{+\infty}\tilde{I}_{n,n+m}(\omega,m\Omega,r)\right)e^{im\Omega t}, \tag{22}$$

where $\tilde{I}_{n,n+m}(\omega,m\Omega,r) = (I'_{n,n+m} + I_{n+m,n})/2$ with

$$I_{n',n}(\omega,\varpi,r) \approx \frac{k_L k'_L C^2}{U_c} J_{n'}\left(k_r r\right) Q_{n,n'}(\omega,\varpi,r), \tag{23}$$

$$Q_{n,n'} = \int_{-\pi}^{\pi} e^{-i(n\gamma-k_r r\sin\gamma)}\Psi_L^\star(K_X,-k_r\sin\gamma,k_C)\Psi_L(K'_X,-k_r\sin\gamma,k'_C)\Phi_{qq}(K_X,-k_r\sin\gamma)\,d\gamma, \tag{24}$$

$$I'_{n,n'}(\omega,\varpi,r) \approx \frac{k_L k'_L C^2}{U_c} J_n\left(k_r r\right) Q'_{n',n}(\omega,\varpi,r), \tag{25}$$

$$Q'_{n',n} = \int_{-\pi}^{\pi} e^{i(n'\gamma-k'_r r\sin\gamma)}\Psi_L^\star(K_X,-k'_r\sin\gamma,k_C)\Psi_L(K'_X,-k'_r\sin\gamma,k'_C)\Phi_{qq}(K'_X,-k'_r\sin\gamma)\,d\gamma, \tag{26}$$

where the primed wavenumbers are a function of frequency $\omega+m\Omega/2$, and the non-primed ones of $\omega-m\Omega/2$, and where

$$\Phi_{qq}(K_X,K_r) = \frac{U_c}{\pi}S_{qq}(\omega)l_S(K_X,K_r), \qquad K_X = K'_X = (\omega-m\Omega/2-n\Omega)/U_c \tag{27}$$

$$k_C = k_z\sin\alpha + (n/r)\cos\alpha, \qquad k'_C = k'_z\sin\alpha + ((n+m)/r)\cos\alpha \tag{28}$$

Time averaged PSD

The time averaged PSD is obtained by retaining mode $m=0$ in equation (22), which gives

$$\overline{S}_{pp}(\mathbf{x_o},\omega) = \frac{S}{\left[8\pi R_e(1-M_z\cos\theta_e)\right]^2}\sum_{n=-\infty}^{+\infty}\tilde{I}_n(\omega,r), \tag{29}$$

$$\tilde{I}_n(\omega,r) = \frac{k_L^2 C^2}{U_c} J_n\left(k_r r\right)\int_{-\pi}^{\pi}\cos\left(n\gamma-k_r r\sin\gamma\right)|\Psi(K_X,-k_r\sin\gamma,k_C)|^2\Phi_{qq}(K_X,-k_r\sin\gamma)\,d\gamma. \tag{30}$$

III. Trailing edge noise formulations for a rotating blade that exlude acceleration effects

A. Instantaneous power spectral density

Following Schlinker and Amiet's approach,[5] the instantaneous PSD is given in source time τ as

$$S_{pp}^{(A)}(\mathbf{x_o}, \tau, \omega) = \left(\frac{\omega'}{\omega}\right)^2 S'_{pp}(\mathbf{X}, \tau, \omega'), \tag{31}$$

where ω' and S'_{pp} are the frequency and the instantaneous power spectral density in the reference frame of the source respectively. The observer position $\mathbf{X}$ is defined as

$$\mathbf{X} = \underline{\mathbf{R_y}}(\alpha)\underline{\mathbf{R_z}}(\pi/2 - \alpha)(\mathbf{x_o} - \mathbf{x_p}), \tag{32}$$

where α is the pitch angle, $\mathbf{x_p} \approx \mathbf{M_{BO}} \mathbf{c_0} \mathbf{T_e}$ is the present source position (assuming that the source is emitted at the hub, which is valid for an observer in the far field) and is expressed in terms of the blade Mach number $\mathbf{M_{BO}} = M_t \hat{\boldsymbol{\gamma}}$ relative to the observer. $\underline{\mathbf{R_z}}$ and $\underline{\mathbf{R_y}}$ denote the rotation matrices about the z-axis and y'-axis respectively, with $y' = \underline{\mathbf{R_z}}(\pi/2 - \alpha)\mathbf{y}$. The propagation time T_e is obtained from $R_e \equiv c_0 T_e$, where R_e is the distance from the convected (or retarded) source position to the observer location:

$$R_e = \frac{R\left(-M_z \cos\Theta + \sqrt{1 - M_z^2 \sin^2\Theta}\right)}{1 - M_z^2}, \quad \text{(far field)}, \tag{33}$$

where $\Theta = \pi - \theta$ denotes the angle between the flow Mach number relative to the observer and $\mathbf{x_o}$ (see figure 1).

Finally, the source frequency ω' is related to the observer frequency ω through the Doppler shift[17]

$$\frac{\omega}{\omega'} = 1 + \frac{\mathbf{M_{BO}} \cdot \widehat{\mathbf{CO}}}{1 + (\mathbf{M_{FO}} - \mathbf{M_{BO}}) \cdot \widehat{\mathbf{CO}}} \quad \text{(far field)}, \tag{34}$$

where $\mathbf{M_{FO}} = -M_z \hat{\boldsymbol{z}}$ is the flow Mach number relative to the observer, and $\widehat{\mathbf{CO}} = \mathbf{CO}/|\mathbf{CO}|$ is the unit vector from the convected source position to the observer position (see figure 1).

The spectrum S'_{pp} in the reference frame of the blade can be computed from equation (1), using a frequency force spectrum S_{ff} representative of a distributed source from equation (3), or a point source as in equation (13).

B. Time averaged power spectral density

The time averaged PSD is obtained by averaging equation (31) over τ, giving

$$\overline{S}_{pp}^{(A)}(\mathbf{x_o}, \omega) = \frac{1}{T}\int_0^T \left(\frac{\omega'}{\omega}\right)^2 S'_{pp}(\mathbf{X}, \tau, \omega')\,\tau. \tag{35}$$

C. Model for the evolution of the acceleration effect

From Lowson,[3] if we ignore the convection effects due to the mean flow, the far field pressure from a rotating dipole is of the form

$$p = \left[\frac{1}{4\pi c_0 R^2 (1-M_n)^2}\dot{\mathbf{x_s}} \cdot \left(\dot{\mathbf{F}} + \frac{\mathbf{F}\dot{M}_n}{1-M_n}\right)\right], \tag{36}$$

where M_n is the source Mach number in the direction of the observer and the square bracket denotes evaluation at the retarded time $\tau = t - R_e/c_0$. Since $\dot{\mathbf{F}}$ varies like $\omega'\mathbf{F}$ and $\dot{M}_n\mathbf{F}$ like $\Omega\mathbf{F}(\hat{\mathbf{r}} \cdot \widehat{\mathbf{CO}})$, the ratio ρ of acceleration term over rectilinear term behaves like

$$\rho = -\frac{\omega}{\Omega}\left(\frac{\omega}{\omega'}\right)^2 M_t \cos\gamma \sin\theta, \tag{37}$$

where $\gamma = \Omega\tau$. For a given frequency ratio ω/Ω, it is not straightforward to predict how the acceleration will affect the instantaneous and time averaged PSDs: it will depend on how the two terms in equation (36) are correlated. However, in the special case $\omega = \Omega$, both terms have the same frequency so the pressure and instantaneous PSDs should behave in a similar manner. We expect ρ to have a "mode shape" that is similar to that of the instantaneous acceleration PSD $S_{pp} - S_{pp}^{(A)}$.

IV. Results

We test the various formulations for two simple models of a propeller blade at cruise and during takeoff. These models were introduced by Blandeau et al[6] and used by Sinayoko et al.[7,8] The parameters are summarized in table 1.

	radius	chord	M_t	α	M_z	M_X
Open propeller at take-off	1.80 m	0.31 m	0.748	13 deg	0.584	0.949
Open propeller at cruise	1.80 m	0.31 m	0.748	38 deg	0.228	0.782

Table 1: Typical parameters[6] for a high speed propeller blade element in take-off and cruise conditions. The span is defined as a third of the radius and the angle of attack is 0. The flow Mach numbers, relative to the observer M_z or to the blade M_X can be obtained from the pitch angle α and the blade Mach M_t but are given for completeness.

A. Time averaged PSD at low and high frequencies

Figures 2 and 3 show the sound pressure level at frequency $\omega = 100\Omega$ for a rotating dipole and a rotating blade element respectively, for the parameters of table 1. In each figure, the formulation that includes the effect of acceleration (equation (21) for a dipole source and equation (29) for a distributed source) is compared to the one that excludes it (equation (35) coupled with the source models of equation (13) for a dipole source and (3) for a distributed source).

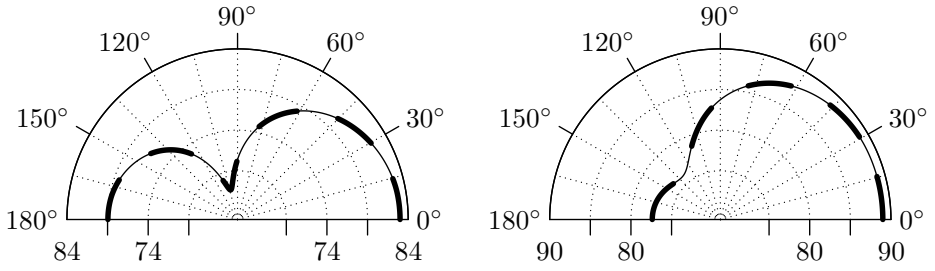

(a) Open propeller at take-off – dipole source (b) Open propeller at cruise – dipole source

Figure 2: Sound pressure level directivity for a rotating dipole based on the exact formulation (equation (29), dashed line) and the approximate formulation (equation (35)). The frequency is $\omega/\Omega = 100$. The decibel scale is relative to 4×10^{-10} and assumes $|\mathbf{x_o}| = 1\,\mathrm{m}$; the wind speed is from right to left.

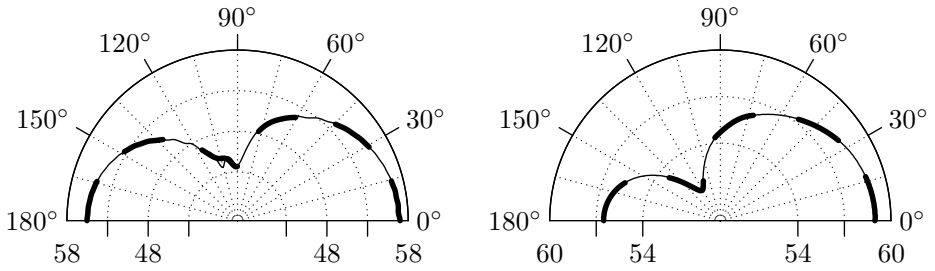

(a) Open propeller at take-off – distributed source (b) Open propeller at cruise – distributed source

Figure 3: Sound pressure level directivity for a rotating blade element for the high frequency formulation (equation (29), dashed line) and the approximate formulation (equation (35)). The frequency is $\omega/\Omega = 100$. The decibel scale is relative to 4×10^{-10} and assumes $|\mathbf{x_o}| = 1\,\mathrm{m}$; the wind speed is from right to left.

B. Sound pressure and sound power error as a function of ω/Ω

Figure 4 shows the evolution of the maximum difference in sound pressure level $|\Delta\mathrm{SPL}|_\infty$ with the frequency ratio ω/Ω, for $0 \leq \theta \leq \pi$, between the formulations that include or exclude the effect of acceleration ($\overline{S}_{pp}$ and $\overline{S}_{pp}^{(A)}$). It is expressed in decibels relative to 4×10^{-10}. The figure also shows how the sound power level

$|\Delta\text{SPWL}|$ varies with the same frequency ratio. The sound power level is computed from:[18]

$$W(\omega) = \frac{\pi R^2}{\rho_0 c_0} \int_0^\pi \overline{S}_{pp}(\theta, \omega) F(\theta) \sin\theta \, d\theta, \qquad F(\theta) = \frac{\beta^4 \sqrt{1 - M_z^2 \sin^2\theta}}{\left(\sqrt{1 - M_z^2 \sin^2\theta} + M_z \cos\theta\right)^2}, \tag{38}$$

and its level in decibels is relative to 1×10^{-12}.

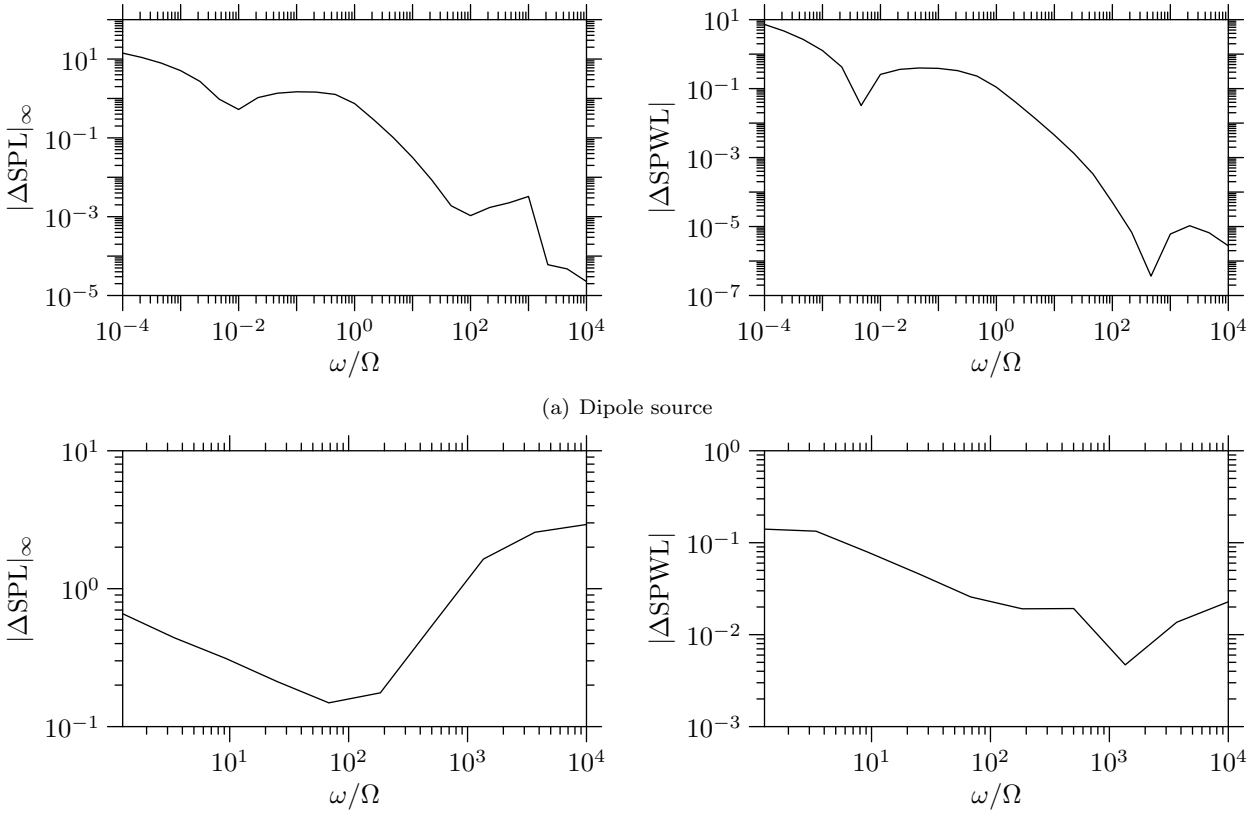

(a) Dipole source

(b) Distributed source

Figure 4: Comparison of the sound pressure (for an observer at $\theta = \pi/6$ and $R = 1$) and sound power levels in dB as a function of frequency ω/Ω from the exact and approximate formulations of equations (21) and (35), for the propeller at cruise point source model.

C. Instantaneous spectra and acceleration effect

Figure 5 shows the instantaneous PSD and the instantaneous PSD due to acceleration during one rotation of the source. The left column compares the instantaneous PSD in dB using the formulations that include or exclude the effect of acceleration. The instantaneous PSD due to acceleration, defined as $S_{pp} - S_{pp}^{(A)}$, is plotted in the right column and is normalized by $\overline{S}_{pp}$. All the spectra are computed assuming a far-field observer in the $(x, z)-$plane at $\theta = \pi/6$ and $R = 1.0$. From top to bottom, each row is associated with a frequency ratio ω/Ω of 0.1, 1.0 or 10.0. For the special case $\omega = \Omega$ (middle row), the instantaneous

acceleration is also compared to the model of equation (37), which predicts the evolution of the acceleration relative to the pressure field for a dipole in rectilinear motion.

V. Discussion

From figure (2), the formulations of equations (21) and (35) for the time averaged PSD radiation from a rotating point source are in excellent agreement at high frequency. As predicted by Amiet, the effect of acceleration becomes negligible at high frequency. Figure (3) demonstrates that this is also true in the case of the rotating source distribution: the formulations of equations (29) and (35) agree to within less than 1 dB. Note that this differs from the result of Sinayoko et al,[7] in which the Doppler shift had been computed incorrectly using the emission source position instead of the convected source position (see equation (34)). The results are also consistent with those of Sinayoko et al.[8]

Figure 4 shows how the agreement between the two approaches (including or excluding the effect of acceleration) varies with the frequency ration ω/Ω. With respect to sound pressure level from a rotating dipole (figure 4(a)), the agreement tends to improve with frequency, for $\times 10^{-4} \leq \omega/\Omega \leq \times 10^{4}$. the two sound pressure levels agree to within 2 dB for $\times 10^{-2} \geq \omega/\Omega$. The agreement is therefore very good down to low unexpectedly low frequencies for all radiation angles. Furthermore, the agreement between the two approaches is even better in terms of sound power level: ΔSPWL $\leq$ 1dB for $0.001 \leq \omega/\Omega \leq 10^{4}$. This is because the effect of acceleration in the plane of the rotor where the sound pressure level is smallest (see the directivities in figure 2). This suggests that, for a rotating dipole, the effect of acceleration remains negligible even when the frequency ω becomes low compared to the rotational speed Ω of the source. This impact becomes significant only at very low frequencies ($\omega/\Omega < 10^{-3}$).

Figure 4(b) suggests that the above result holds to a certain extent for the distributed source model: ΔSPWL $\leq$ 0.2dB for $1 \leq \omega/\Omega \leq 10^{4}$. The model of Schlinker and Amiet, which neglects the effect of acceleration, holds even when the frequency is comparable to Ω. Note that it has not been possible to explore lower frequencies ($\omega \ll \Omega$) because equation (22) assumes that ω does not tend to 0.

Until now, the approach of Schlinker and Amiet was thought to be limited to frequencies satisfying $\omega \gg \Omega$. The above results suggest that it holds down to much lower frequencies, at least down to $\omega = \Omega$. To explain this result, the evolution of the instantaneous PSD was plotted in figures 5 and 6 for a rotating dipole source and a rotating distributed source respectively. At high frequency ($\omega = 10\Omega$, figure 5(c) left), the maximum amplitude of the acceleration term is less than 0.25 dB compared to 84.8 dB for the time averaged PSD. The impact of acceleration steadily increases as ω/Ω decreases, up to 1 dB at $t = 0.8T$ for $\omega/\Omega = 0.1$ (figure 5(a) left). However, the effect of the acceleration term is on average 0 as can be seen in the right column of figure 5. Thus, even though its amplitude is no longer negligible at low frequencies, it's effect

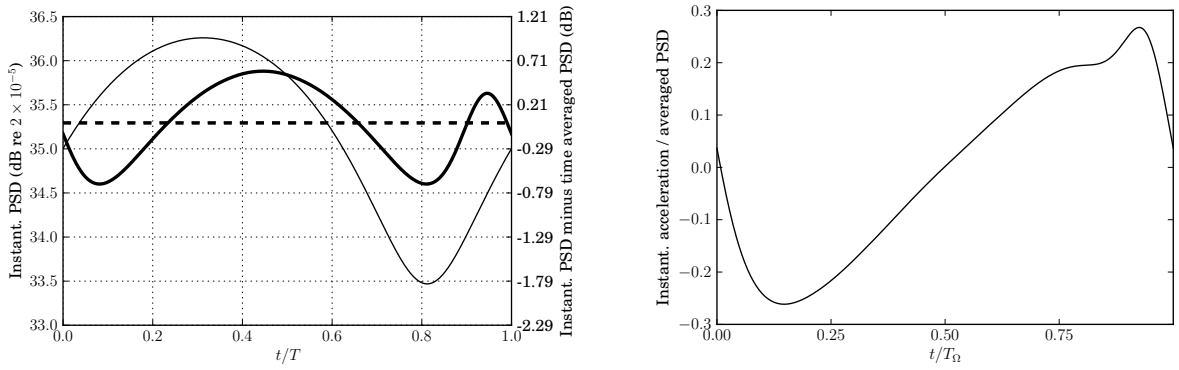

(a) Power spectral densities (left) and acceleration effect (right) for $\theta = \pi/6$ and $\omega/\Omega = 0.1$

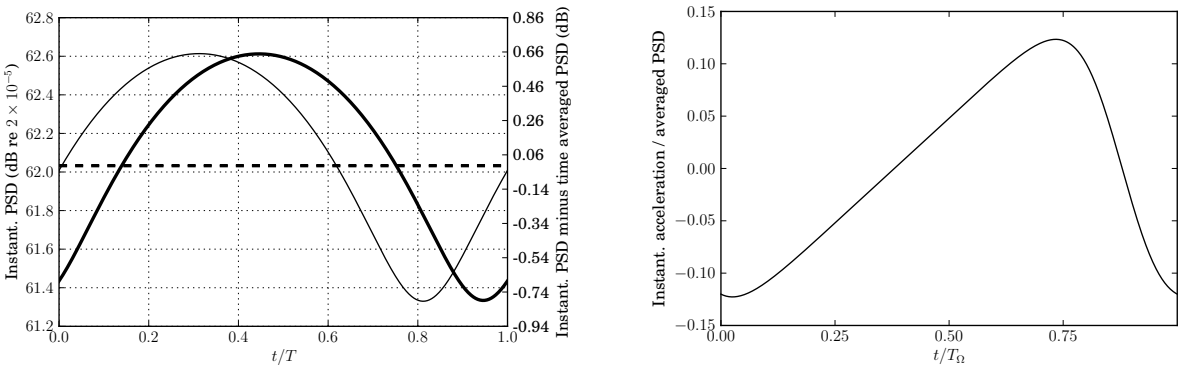

(b) Power spectral densities (left) and acceleration effect (right) for $\theta = \pi/6$ and $\omega/\Omega = 1$

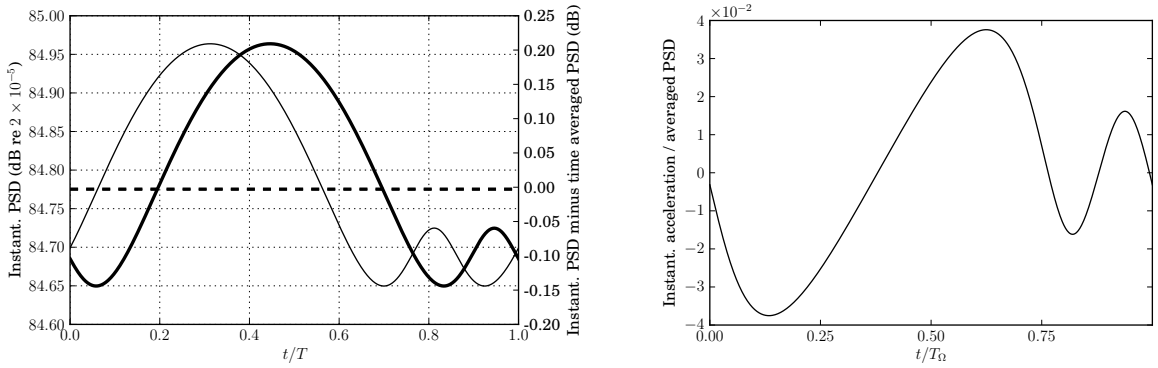

(c) Power spectral densities (left) and acceleration effect (right) for $\theta = \pi/6$ and $\omega/\Omega = 10$

Figure 5: Comparison of the instantaneous pressure PSD over one period T_Ω for a rotating dipole from the exact and approximate formulations of equations (20) and (31), using the model of a propeller at cruise with an observer at $\theta = \pi/6$ and $R = 1$. Left figure: the left axis shows the amplitude of the instantaneous PSD in dB; the right axis shows the difference in dB between the instantaneous PSD and the time averaged PSD; the time averaged PSDs are shown in dashed lines and the instantaneous PSDs in solid lines, with the thick lines representing the PSDs from the exact formulation that includes the effect of acceleration, while the thin lines represent the PSDs from the approximate formulation that excludes the effect of acceleration. Right figure: acceleration effect in dB measured as the difference between the the instantaneous PSDs from the exact and approximate approaches (the two solid curves in the left figure).

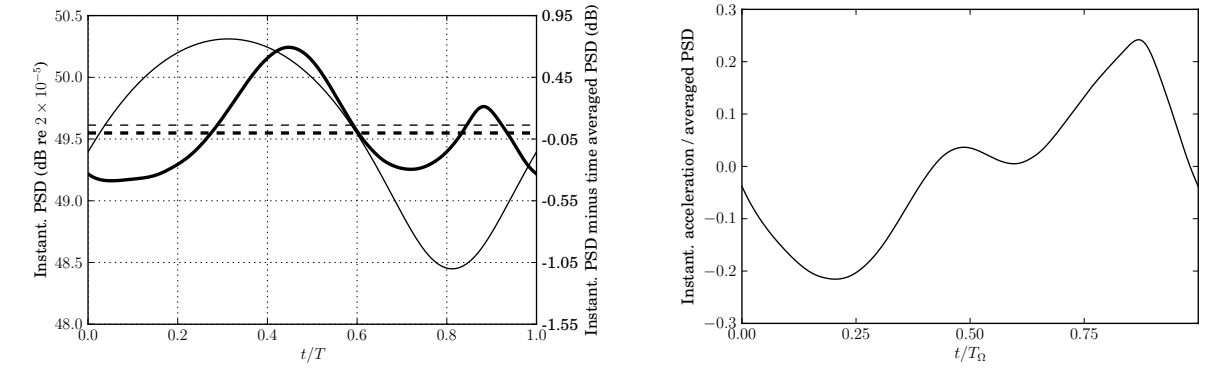

(a) Power spectral densities (left) and acceleration effect (right) for $\theta = \pi/6$ and $\omega/\Omega = 0.1$

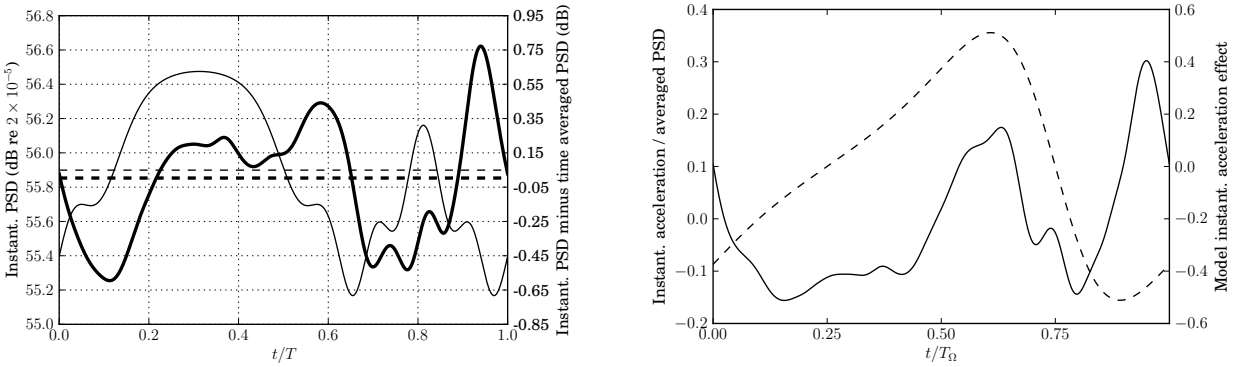

(b) Power spectral densities (left) and acceleration effect (right) for $\theta = \pi/6$ and $\omega/\Omega = 1$

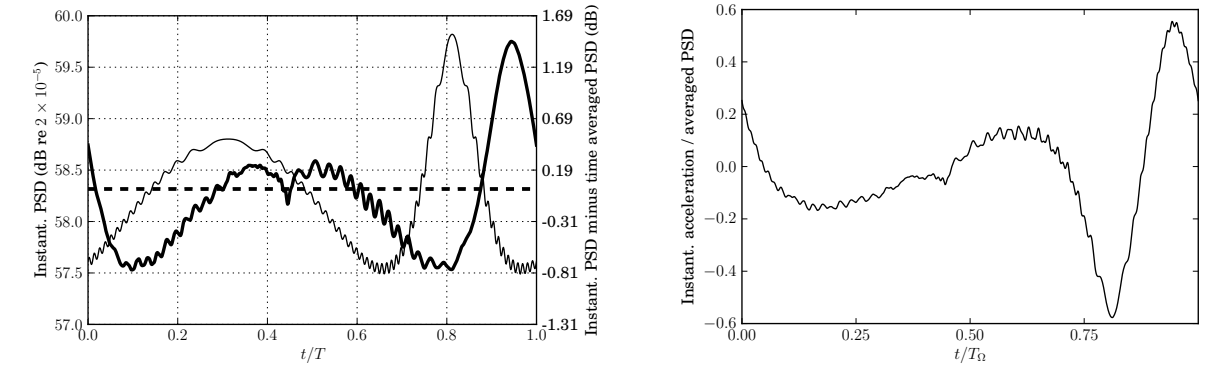

(c) Power spectral densities (left) and acceleration effect (right) for $\theta = \pi/6$ and $\omega/\Omega = 10$

Figure 6: Comparison of the instantaneous pressure PSD over one period T_Ω for a rotating blade blade element from the exact and approximate formulations of equations (21) and (31), using the model of a propeller at cruise with an observer at $\theta = \pi/6$ and $R = 1$. Left figure: the left axis shows the amplitude of the instantaneous PSD in dB; the right axis shows the difference in dB between the instantaneous PSD and the time averaged PSD; the time averaged PSDs are shown in dashed lines and the instantaneous PSDs in solid lines, with the thick lines representing the PSDs from the exact formulation that includes the effect of acceleration, while the thin lines represent the PSDs from the approximate formulation that excludes the effect of acceleration. Right figure: acceleration effect in dB measured as the difference between the the instantaneous PSDs from the exact and approximate approaches (the two solid curves in the left figure).

on the time averaged PSD remains negligible. This explains why the thin and thick dashed lines in the left column of figure 5, which represent the time averaged PSDs from the exact and approximate formulations, are identical.

In the special case $\omega = \Omega$, the simple model of equation (37) appears to predict the evolution of the acceleration term. Since $\cos\gamma$ averages out to 0 over one rotation, that equation also suggests that the effect of acceleration averages out to 0. Nevertheless, this piece of evidence is qualitative and more research is needed to explain why the acceleration of the source averages out to 0 and therefore has little impact on the average PSD.

From figure 6, we have also been able to predict the instantaneous spectrum radiating from a rotating distributed source based on Amiet's trailing edge noise blade response function. Apart from a phase shift, the instant PSDs from equations (22) and (31) are in agreement at $\omega = 10\Omega$ (figure 6(c)). The amplitude of the acceleration does not decay to 0 when ω/Ω increases (figure 6(a-c)), but its average does tend to 0 (the two dashed lines representing the averaged PSDs overlap in 6(c)). At lower frequencies, the average of the acceleration term is non-zero but it remains very small at less than 0.5 dB. This suggests that acceleration has little effect on the time averaged PSD for a distributed source even at low frequencies relative to Ω.

Conclusions

For a rotating dipole, the effect of acceleration is negligible not just when $\omega \gg \Omega$ but over a much wider frequency range: the impact of the acceleration on the sound power level was found to be below 1 dB for $10^{-3} \leq \omega/\Omega \leq 10^4$. This suggest that, in the far field, it is acceptable to neglect the effect of acceleration for computing the average sound power level radiating from a rotating dipole. The result appears to hold also in the case of a distributed source based on Amiet's[1] blade response function, although it has not been possible to investigate frequencies much smaller than the angular velocity Ω of the rotor.

The effect of acceleration has been explored by examining the impact of the acceleration on the instantaneous power spectra density. Although acceleration was found to amplify or decrease the instantaneous power spectral density by several decibels at low frequencies, its impact was found to be 0 on average, over one rotation of the rotor blade.

This paper has corrected an erroneous result presented by Sinayoko et al;[7] the approach of Schlinker and Amiet[5] is now found to be applicable to subsonic blade elements rotating even at high speed ($M_X = 0.95$). It can therefore be used to estimate trailing edge noise from open rotor blades.

Although this paper has dealt with trailing edge noise, the conclusions are likely to hold for other sources of airfoil noise, such as leading edge noise.

Acknowledgements

Samuel Sinayoko and Anurag Agarwal wish to acknowledge the support of Mitsubishi Heavy Industries. Mike Kingan wishes to acknowledge the continuing financial support provided by Rolls-Royce plc. through the University Technology Centre in Gas Turbine Noise at the Institute of Sound and Vibration Research. The authors thank Michel Roger and Stephane Moreau for their feedback on the early version of this paper.

References

[1]Amiet, R., "Noise due to turbulent flow past a trailing edge," *Journal of Sound and Vibration*, Vol. 47, No. 3, Aug. 1976, pp. 387–393.

[2]Amiet, R. K., "High frequency thin-airfoil theory for subsonic flow," *AIAA Journal*, Vol. 14, 1976, pp. 1076–1082.

[3]Lowson, M. V., "The Sound Field for Singularities in Motion," *Proceedings of the Royal Society A: Mathematical, Physical and Engineering Sciences*, Vol. 286, No. 1407, Aug. 1965, pp. 559–572.

[4]Amiet, R. K., "Leading and Trailing Edge Noise from a Helicopter Rotor," Tech. rep., UTRC Report 86-53, 1986.

[5]Schlinker, R. H. and Amiet, R. K., "Helicopt," Tech. Rep. 1, NASA Contractor Report 3470, Jan. 1981.

[6]Blandeau, V. and Joseph, P., "Validity of Amiets Model for Propeller Trailing-Edge Noise," *AIAA Journal*, Vol. 49, No. 5, May 2011, pp. 1057–1066.

[7]Sinayoko, S., Kingan, M., and Agarwal, A., "Trailing edge noise prediction for rotating blades: analysis and comparison of two classical approaches," *AIAA paper 2012-2302*, 2012, pp. 1–20.

[8]Sinayoko, S., Kingan, M., and Agarwal, A., "Trailing edge noise theory for rotating blades in uniform flow," *ArXiv e-prints*, April 2013.

[9]Antoni, J., "Cyclostationarity by examples," *Mechanical Systems and Signal Processing*, Vol. 23, No. 4, 2009, pp. 9871036.

[10]Amiet, R., "Effect of the incident surface pressure field on noise due to turbulent flow past a trailing edge," *Journal of Sound and Vibration*, Vol. 57, 1978, pp. 305–306.

[11]Amiet, R., "Acoustic radiation from an airfoil in a turbulent stream," *Journal of Sound and Vibration*, Vol. 41, No. 4, Aug. 1975, pp. 407–420.

[12]Roger, M. and Moreau, S., "Back-scattering correction and further extensions of Amiet's trailing-edge noise model. Part 1: theory," *Journal of Sound and Vibration*, Vol. 286, No. 3, Sept. 2005, pp. 477–506.

[13]Brooks, T. F. and Hodgson, T. H., "Trailing edge noise prediction from measured surface pressures," *Journal of Sound and Vibration*, Vol. 78, 1981, pp. 69–117.

[14]Kim, Y. N. and George, a. R., "Trailing-Edge Noise from Hovering Rotors," *AIAA Journal*, Vol. 20, No. 9, Sept. 1982, pp. 1167–1174.

[15]Blandeau, V., *Aerodynamic Broadband Noise from Contra-Rotating Open Rotors*, Ph.D. thesis, University of Southampton, 2011.

[16]Chou, S. and George, A. R., "Effect of angle of attack on rotor trailing-edge noise," *AIAA journal*, Vol. 22, 1984, pp. 1821–1823.

[17]Amiet, R. K., "Frame of Reference Considerations for the Forward Flight Noise Problem," Tech. rep., UARL Report N212775-1, 1974.

[18]Sinayoko, S., Joseph, P., and McAlpine, A., "Multimode radiation from an unflanged, semi-infinite circular duct with uniform flow," *The Journal of the Acoustical Society of America*, Vol. 127, 2010, pp. 2159.

A. Results for a wind turbine blade element

B. Results for a cooling fan blade element

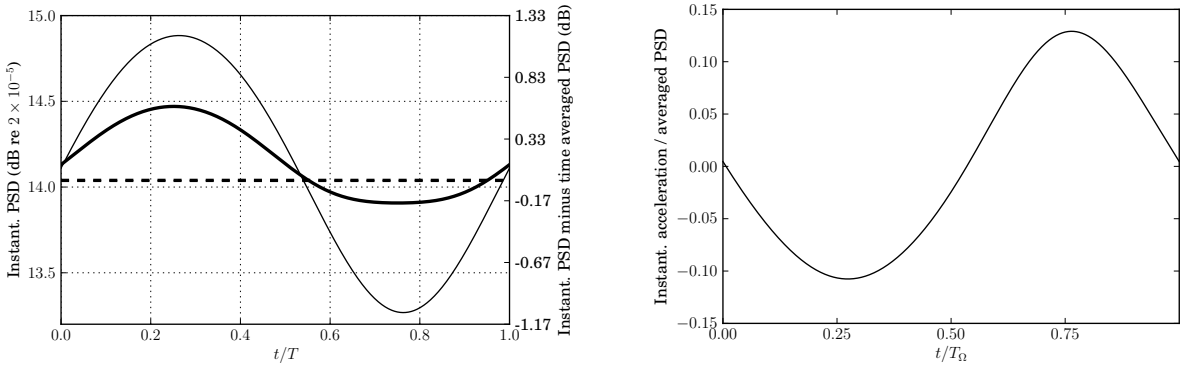

(a) Power spectral densities (left) and acceleration effect (right) for $\theta = \pi/6$ and $\omega/\Omega = 0.1$

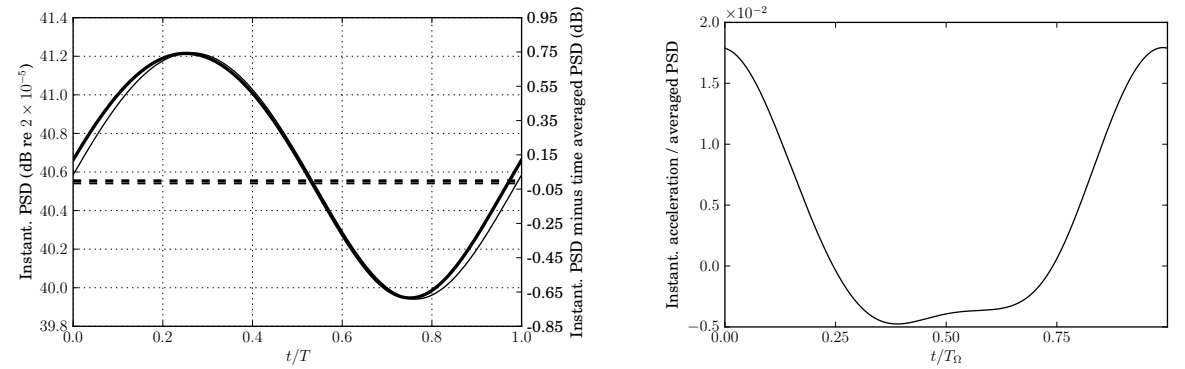

(b) Power spectral densities (left) and acceleration effect (right) for $\theta = \pi/6$ and $\omega/\Omega = 1$

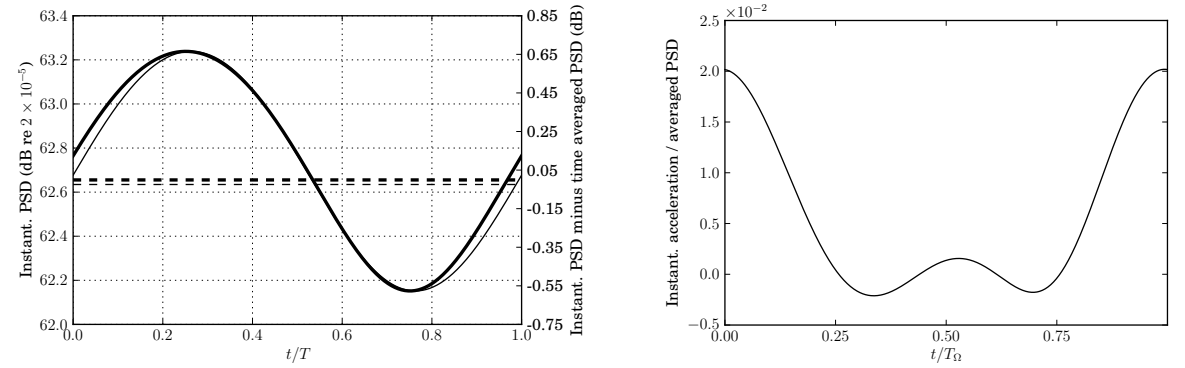

(c) Power spectral densities (left) and acceleration effect (right) for $\theta = \pi/6$ and $\omega/\Omega = 10$

Figure 7: Comparison of the instantaneous pressure PSD over one period T_Ω for a rotating dipole from the exact and approximate formulations of equations (20) and (31), using the model of a wind turbine with an observer at $\theta = \pi/6$ and $R = 1$. Left figure: the left axis shows the amplitude of the instantaneous PSD in dB; the right axis shows the difference in dB between the instantaneous PSD and the time averaged PSD; the time averaged PSDs are shown in dashed lines and the instantaneous PSDs in solid lines, with the thick lines representing the PSDs from the exact formulation that includes the effect of acceleration, while the thin lines represent the PSDs from the approximate formulation that excludes the effect of acceleration. Right figure: acceleration effect in dB measured as the difference between the the instantaneous PSDs from the exact and approximate approaches (the two solid curves in the left figure).

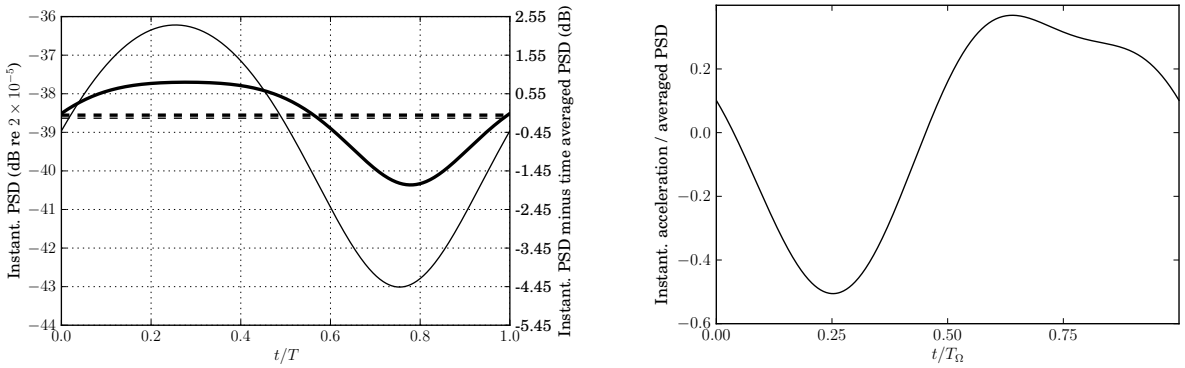

(a) Power spectral densities (left) and acceleration effect (right) for $\theta = \pi/6$ and $\omega/\Omega = 0.1$

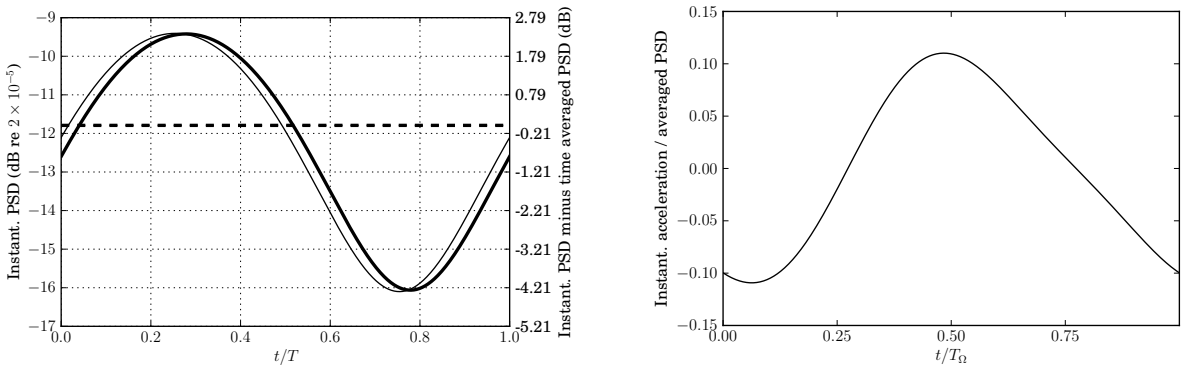

(b) Power spectral densities (left) and acceleration effect (right) for $\theta = \pi/6$ and $\omega/\Omega = 1$

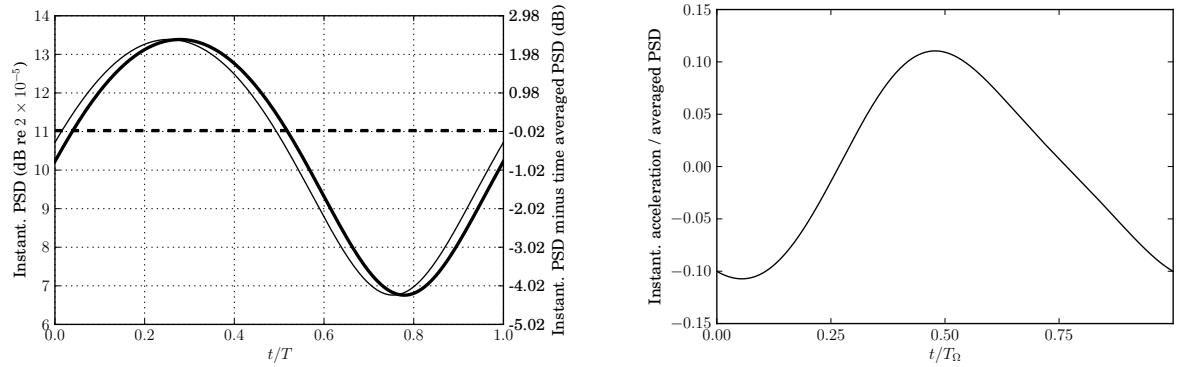

(c) Power spectral densities (left) and acceleration effect (right) for $\theta = \pi/6$ and $\omega/\Omega = 10$

Figure 8: Comparison of the instantaneous pressure PSD over one period T_Ω for a rotating dipole from the exact and approximate formulations of equations (20) and (31), using the model of a wind turbine with an observer at $\theta = \pi/6$ and $R = 1$. Left figure: the left axis shows the amplitude of the instantaneous PSD in dB; the right axis shows the difference in dB between the instantaneous PSD and the time averaged PSD; the time averaged PSDs are shown in dashed lines and the instantaneous PSDs in solid lines, with the thick lines representing the PSDs from the exact formulation that includes the effect of acceleration, while the thin lines represent the PSDs from the approximate formulation that excludes the effect of acceleration. Right figure: acceleration effect in dB measured as the difference between the the instantaneous PSDs from the exact and approximate approaches (the two solid curves in the left figure).

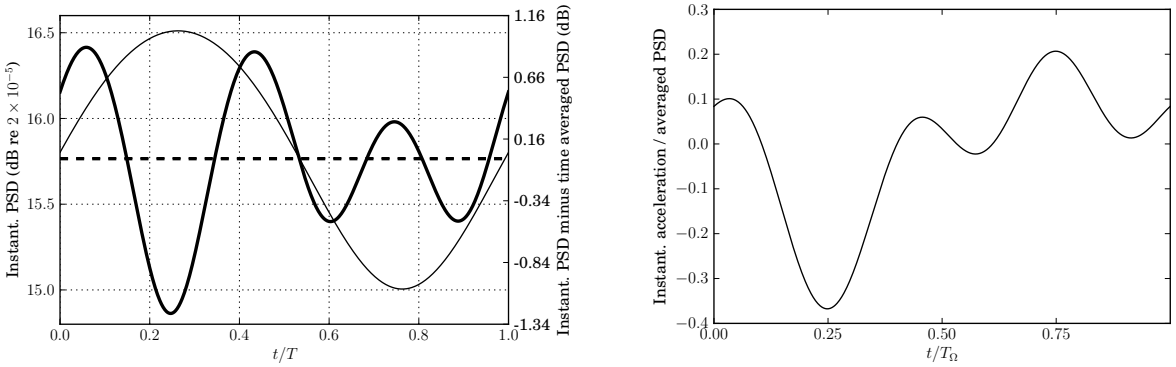

(a) Power spectral densities (left) and acceleration effect (right) for $\theta = \pi/6$ and $\omega/\Omega = 0.1$

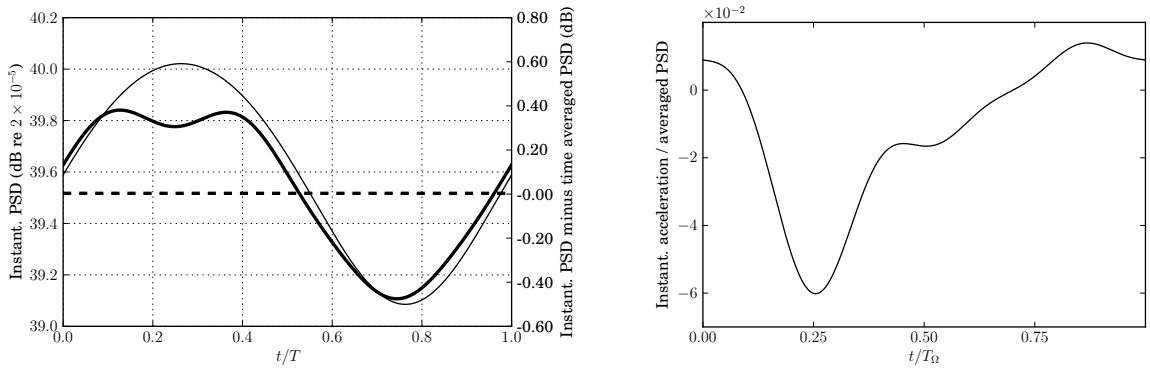

(b) Power spectral densities (left) and acceleration effect (right) for $\theta = \pi/6$ and $\omega/\Omega = 1$

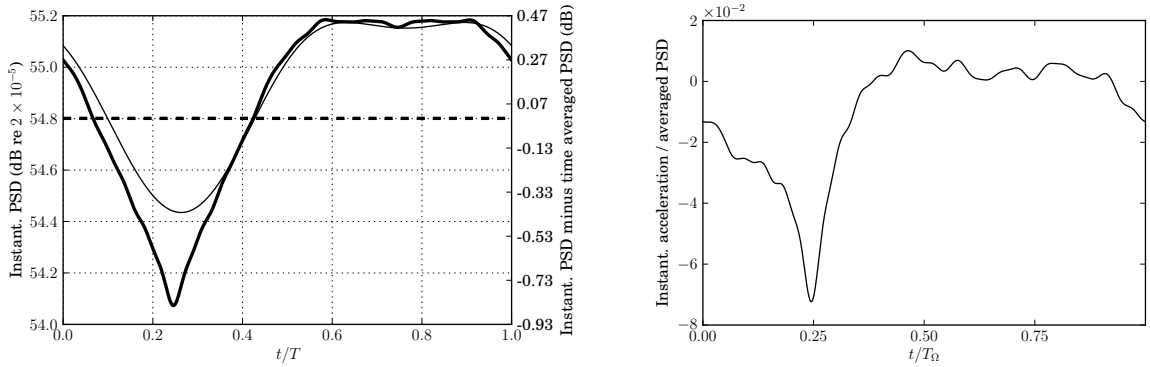

(c) Power spectral densities (left) and acceleration effect (right) for $\theta = \pi/6$ and $\omega/\Omega = 10$

Figure 9: Comparison of the instantaneous pressure PSD over one period T_Ω for a rotating blade blade element from the exact and approximate formulations of equations (21) and (31), using the model of a wind turbine with an observer at $\theta = \pi/6$ and $R = 1$. Left figure: the left axis shows the amplitude of the instantaneous PSD in dB; the right axis shows the difference in dB between the instantaneous PSD and the time averaged PSD; the time averaged PSDs are shown in dashed lines and the instantaneous PSDs in solid lines, with the thick lines representing the PSDs from the exact formulation that includes the effect of acceleration, while the thin lines represent the PSDs from the approximate formulation that excludes the effect of acceleration. Right figure: acceleration effect in dB measured as the difference between the the instantaneous PSDs from the exact and approximate approaches (the two solid curves in the left figure).

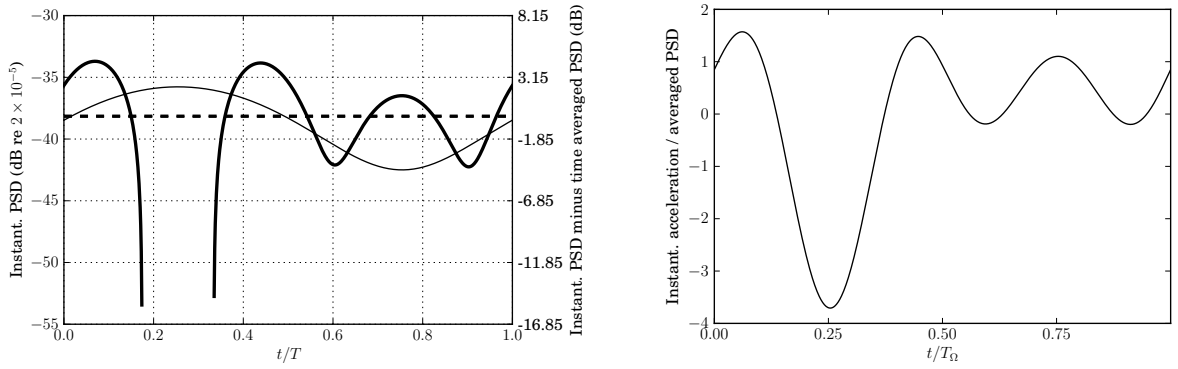

(a) Power spectral densities (left) and acceleration effect (right) for $\theta = \pi/6$ and $\omega/\Omega = 0.1$

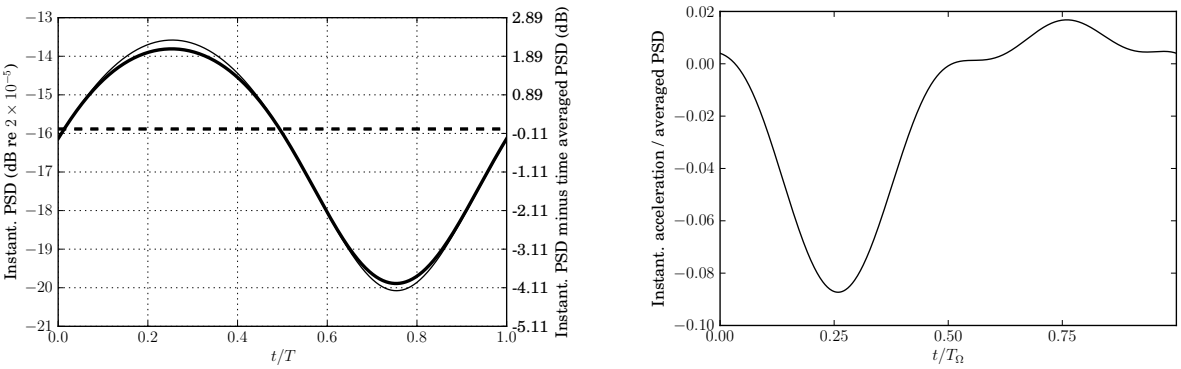

(b) Power spectral densities (left) and acceleration effect (right) for $\theta = \pi/6$ and $\omega/\Omega = 1$

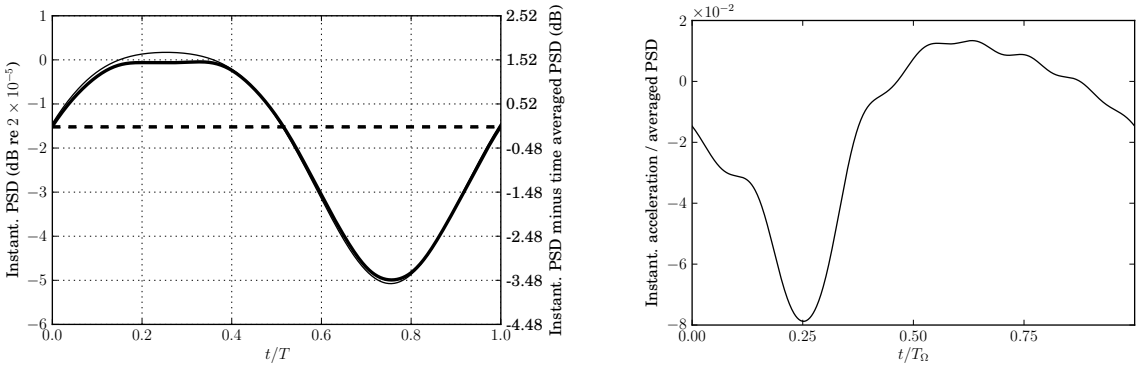

(c) Power spectral densities (left) and acceleration effect (right) for $\theta = \pi/6$ and $\omega/\Omega = 10$

Figure 10: Comparison of the instantaneous pressure PSD over one period T_Ω for a rotating blade blade element from the exact and approximate formulations of equations (21) and (31), using the model of a cooling fan with an observer at $\theta = \pi/6$ and $R = 1$. Left figure: the left axis shows the amplitude of the instantaneous PSD in dB; the right axis shows the difference in dB between the instantaneous PSD and the time averaged PSD; the time averaged PSDs are shown in dashed lines and the instantaneous PSDs in solid lines, with the thick lines representing the PSDs from the exact formulation that includes the effect of acceleration, while the thin lines represent the PSDs from the approximate formulation that excludes the effect of acceleration. Right figure: acceleration effect in dB measured as the difference between the the instantaneous PSDs from the exact and approximate approaches (the two solid curves in the left figure).